Reversible Membrane Pearling in Live Cells upon Destruction of the Actin Cortex

Doris Heinrich,[†‡] Mary Ecke,[§] Marion Jasnin,[§] Ulrike Engel,[¶] and Günther Gerisch[§*]
[†]Leiden Institute of Physics, LION, Leiden University, The Netherlands; [‡]Fraunhofer-Institut für Silicatforschung ISC, Würzburg, Germany; [§]Max Planck Institute of Biochemistry, Martinsried, Germany; and [¶]Nikon Imaging Center, Heidelberg, Germany

ABSTRACT Membrane pearling in live cells is observed when the plasma membrane is depleted of its support, the cortical actin network. Upon efficient depolymerization of actin, pearls of variable size are formed, which are connected by nanotubes of ~40 nm diameter. We show that formation of the membrane tubes and their transition into chains of pearls do not require external tension, and that they neither depend on microtubule-based molecular motors nor pressure generated by myosin-II. Pearling thus differs from blebbing. The pearling state is stable as long as actin is prevented from polymerizing. When polymerization is restored, the pearls are retracted into the cell, indicating continuity of the membrane. Our data suggest that the alternation of pearls and strings is an energetically favored state of the unsupported plasma membrane, and that one of the functions of the actin cortex is to prevent the membrane from spontaneously assuming this configuration.

INTRODUCTION

The shape of the plasma membrane in a motile eukaryotic cell is normally dominated by the organization of the actin network in the cell cortex, which is linked by noncovalent bonds to the lipid bilayer on the cell surface. In cooperation with associated proteins, the actin network forces the membrane to bend, forming protrusions of different shapes like lamellipodia and filopodia, or invaginations like phagosomes and other endocytic vesicles. The question addressed here is how the complex membrane of a living cell self-organizes when support by the submembraneous actin layer is impaired.

The scenario we study is as follows. The highly motile cells of *Dictyostelium discoideum* rapidly change shape and efficiently internalize plasma membrane by endocytosis. Osmotic pressure in the cells is regulated through the outward pumping of water by contractile vacuoles that periodically form a channel to the plasma membrane (1), thus keeping cell volume within narrow limits. Both the irregular and variable shape of migrating cells and endocytic activity depend on the availability of membrane area. We challenged the regulation of surface area by a blocker of actin polymerization, latrunculin A (latA), at concentrations that still allow the contractile vacuoles to work as osmoregulators. Because phagocytosis, macropinocytosis, as well as endocytosis of clathrin-coated vesicles (2) are arrested at the latA concentrations used, the internalization of excess membrane is prevented. Under these conditions, the cells round up without expanding their volume. The excess membrane has been observed to fold under these conditions into tubes, which are converted into chains of interconnected pearls in *Dictyostelium* (3) as in mammalian cells (4).

Shape variations in model membranes have been studied in giant unilamellar vesicles (GUVs) (5). In GUVs composed of defined multicomponent lipid mixtures and also in plasma membrane vesicles lacking an underlying cytoskeleton, lipids and proteins can segregate into two fluid phases, a liquid phase with short-range order (L_0) and a liquid-disordered (L_d) phase (6,7). This separation of phases occurs at temperatures below a mixing point, and is typical of systems that are destabilized by competing interactions (8). The segregated domains differ in lipid composition and may also differ in membrane curvature. The coupling between segregation and curvature has two aspects: 1), segregation can be induced by fluctuations in local membrane curvature (9); and 2), segregation results in stabilizing the membrane in its curved state (10).

Even in uniform GUVs that consist only of one type of lipid, local shape differences can be induced by applying external force. Nanotubes can be extracted from a GUV by axial strain (11). Close to natural conditions, nanotubes are extracted by the activity of microtubule-dependent motor proteins (12–14). The use of nonprocessive motors showed that these nanotubes persist only under the continuous application of force, because they retract when the motors dissociate (15).

Local pulling force applied through a laser tweezer may cause a membrane tube to transform into pearls on a string. Dynamic pearling states can be set off in tubes composed of a single lipid (16). This long-range, slowly relaxing Rayleigh-like instability is due to the competition of curvature energy and surface tension. Pearling can also be induced in the absence of a pulling force. Thread-like oleate vesicles are induced to pearl by the photooxidation of thiols, probably causing a change in surface tension (17), and pearls on a chain can be generated by the absorbance of cationic nanoparticles to the inner leaflet of

Submitted July 29, 2013, and accepted for publication December 11, 2013.
*Correspondence: gerisch@biochem.mpg.de
Editor: Cecile Sykes.

0006-3495/14/03/1079/13 $2.00
http://dx.doi.org/10.1016/j.bpj.2013.12.054

DOPC (dioleoyl-glycero-phosphocholine) vesicles (18) or by increasing the osmotic pressure within a tube (19).

The study of membrane pearling in live cells has been pioneered by Bar-Ziv et al. (4). These authors discovered pearling in membrane tubes that were under tension, which was supplied by local attachment of the tubes to a solid substrate. If the rigidity of the submembraneous actin shell is reduced by partial depolymerization, the membrane tubes are converted into pearls on a chain.

Here, we explore the transformation of the plasma membrane of live cells into tubes and pearls, and the reversal of this transformation upon reconstitution of the actin cortex. A distinguishing feature of the pearling studied by us is its independence of tension exerted by stretching the membrane tubes between adhesion points, as evidenced by the pearl formation on free, unattached portions of the cell surface. We show that membrane pearling in *Dictyostelium* cells does not require force generation by microtubule-based motors. Moreover, the pearling is independent of internal pressure generated by myosin-II, and is thus distinguished from blebbing.

By cryo-electron tomography (cryo-ET) we show the persistence of short bundles of actin filaments in pearls formed in the presence of 5 μM latA and the absence of filaments in tubes or pearls after the depolymerization of actin at 30 μM latA. We discuss pearling as a process of membrane self-organization, which is prevented by an intact actin network in the cell cortex.

MATERIALS AND METHODS

Strains, treatment of cells, and imaging conditions

Cells of *D. discoideum* strain AX2-214 that expressed various fluorescent proteins were cultivated at 21–23°C in nutrient medium supplemented with appropriate selection markers. The cells expressed LimEΔ-GFP (20), GFP-α-tubulin (21), the PH-domain of human phospholipase Cδ1 (22), GFP-coronin (22), or free GFP. In the AX2-derived myosin II-HC deficient mutant strain HS2205 (23), mRFPM-LimEΔ (24) was expressed. For confocal fluorescence imaging, the cells were washed in 17 mM Na/K phosphate buffer, pH 6.0, and transferred into an open chamber on a glass coverslip. LatA (Life Technologies, Grand Island, NY) was routinely used at 5 or 10 μM, and was increased to 30 μM for the efficient depolymerization of actin. To induce blebbing, cells were incubated with 50 or 100 μM 2,4-dinitrophenol (Sigma-Aldrich, St. Louis, MO).

For labeling of the plasma membrane, 0.25 μg/ml of FM4–64 (Life Technologies) were added (diluted 1:4000 from a stock solution of 1 mg/ml in dimethyl sulfoxide (DMSO)). For membrane labeling in combination with concanavalin A (ConA) (Life Technologies) treatment, cells were first incubated for 1 h in the cold in phosphate buffer at pH 8.0 with 50 μM Alexa Fluor 568 succinimidyl ester (Life Technologies), diluted from a stock solution of 1 mg in 250 μl DMSO. Subsequently, the cells were treated for 10 min with 10 μM latA at room temperature. After removal of the latA, 50 μg/ml of ConA-FITC (Life Technologies) were added.

Most confocal images were acquired with a Zeiss LSM 780 equipped with a Plan-APO 63×/NA1.46 oil immersion objective (Carl Zeiss Microscopy GmbH, Jena, Germany), those in Fig. 1 *B* and Fig. 2 *A* at a Nikon Eclipse TE 300 microscope equipped with a 100×/1.4 NA oil PlanApo objective (Nikon, Tokyo, Japan), in combination with an Ultra View confocal scanner (Perkin Elmer, Waltham, MA) and an Orca ERC4742-95-12 ERG camera (Hamamatsu Photonics, Hamamatsu, Japan). Images of Fig. 5 were obtained using an Ultra View system (Perkin Elmer) on a Nikon TE-2000 microscope equipped with a VC 100×/1.4 NA PlanApo objective (Nikon, Tokyo, Japan) and an EM-CCD camera (Andor Technology, Belfast, UK). For the 3D reconstructions (see Fig. 5, *A–C*), *z*-stacks generated with a spacing of 0.3 μm were deconvolved using Huygens Essential 3.0.0 (Scientific Volume Imaging, 1213 VB Hilversum, The Netherlands) and surface rendered using Volocity 3.7.0 (Perkin Elmer). The equipment for total internal reflection fluorescence microscopy has been described in (2).

Fluorescence recovery after photobleaching (FRAP) experiments were performed using an Olympus IX 81 microscope with a 60×/1.35 NA oil UPlanSApo objective (Olympus, Tokyo, Japan), a Yokogawa spinning-disc scan head CSU_X1 (Andor Technology, Belfast, UK), an IQ version 1.9 FRAPPA configuration (Andor Technology), and an IXON DU897_BV_3880-iXon plus camera (Andor Technology). For bleaching, an ALC laser combined with a 488 nm/50 mW Coherent Sapphire laser (Andor Technology) was used.

Cryo-ET

Cells were plated on glow-discharged, holey-carbon-film-coated gold EM grids (C-flat 2/1-2Au, Protochips, Raleigh, NC) and kept for 2 h, before the cells were treated with 5 or 30 μM latA for 15 min. For cryo-preparation we added BSA-coated 15 nm colloidal gold (Aurion, Wageningen, The Netherlands) on top of the grid, removed excess liquid by blotting from the reverse side, and rapidly plunge-froze the grids in liquid propane-ethane.

Tomograms were obtained under low-dose conditions using a Tecnai G2 Polara transmission electron microscope (FEI, Eindhoven, The Netherlands) equipped with a 300-kV field emission gun, a Gatan GIF 2002 post-column energy filter, and a 2048 × 2048 slow-scan CCD camera (Gatan, Pleasanton, CA). The electron microscope was operated at an accelerating voltage of 300 kV; the pixel size at the specimen level was 0.713 nm. Tilt series were recorded using the SerialEM software (25), typically covering an angular range from $-60°$ to $+60°$ with a tilt increment of 2°, defocus values of -6 and -12 μm, and a total electron dose of 200 electrons /Å^2. The projection images were aligned using the gold beads as fiducial markers. Tomograms with a once binned pixel size of 1.42 nm were calculated using the software IMOD (26).

For automated filament segmentation, tomograms were subjected to nonlocal means filtering. Actin filaments were traced using an automated segmentation algorithm implemented in the Amira software (27), using a generic filament as a template (28). Diameter and length of the generic filament were 8 and 42 nm, respectively; short filamentous structures of <60 nm lengths were filtered out to reduce background noise. To increase contrast in the slices (see Fig. 1 *D* and Fig. 3), four slices were summed up in the *z* direction.

RESULTS

Removal of the actin network transforms plasma membrane into two coexisting states

To visualize membrane pearling in cells of *D. discoideum*, we have labeled filamentous actin with LimEΔ-GFP (20) and the plasma membrane with the red fluorescent styryl dye FM4-64. The double-labeled cells were subjected to confocal imaging (Fig. 1 *A*). Membrane pearling was reproducibly induced by the depolymerization of actin using

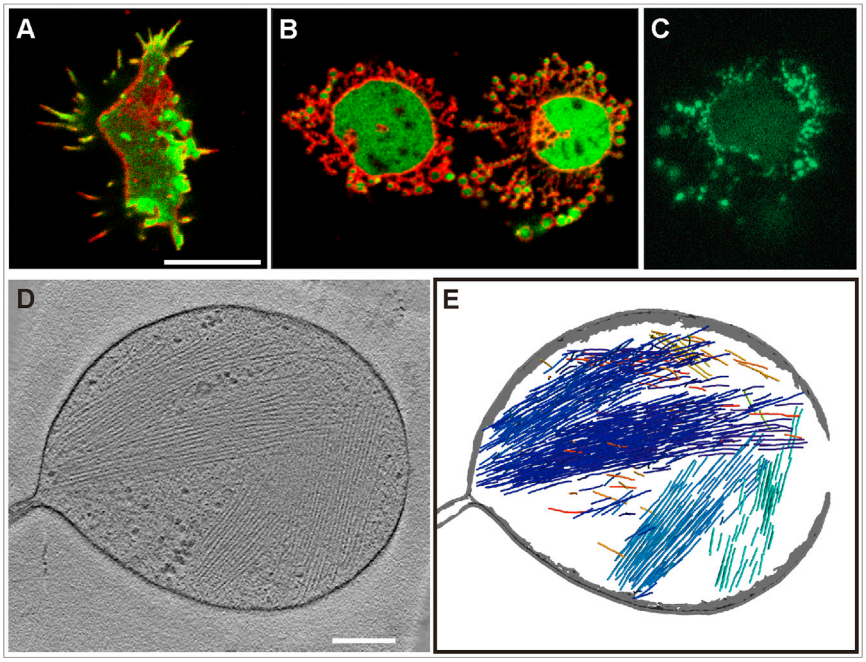

FIGURE 1 Membrane pearling and destruction of the actin cortex in response to actin depolymerization. (*A* and *B*) Confocal images of an untreated cell of *D. discoideum* (*A*) and of cells incubated with 5 μM latA (*B*). The cells expressed LimEΔ-GFP as a label for filamentous actin (*green*) and were stained with FM4-64, which integrates into the plasma membrane and from there into the membranes of the contractile vacuole system (*red*). In the motile cell of (*A*), actin is assembled along the filopodia and in the cortical region beneath the plasma membrane. In the two cells of (*B*) showing extensive membrane pearling, the LimEΔ-GFP is dispersed in the cytoplasm and the lumen of the pearls. A time series of pearling in the cell displayed in (*A*) is shown in Movie S1. (*C*) Coronin, a protein preferentially associated with disassembling actin filaments (22), is enriched in the pearls. The cell expressing GFP-coronin has been imaged by total internal reflection fluorescence microscopy. (*D* and *E*) A pearl subjected to cryo-ET, showing bundles of actin filaments in its interior. The cell was treated for 15 min with 5 μM latA. In (*D*) a slice through the tomogram is displayed. Segmentation of the filaments and the membrane is shown in (*E*). Bar for (*A–C*) 10 μm; for (*D* and *E*) 200 nm. The tomogram is shown in Movie S2.

5 μM latA. Under these conditions, the microtubule-dependent motility of intracellular vesicles is not disturbed and may even be enhanced (29). The contractile vacuoles continue to pulse, indicating that their osmoregulatory activity is preserved.

After the addition of latA, the leading edges became indistinguishable, and actin-based cell-surface protrusions such as filopodia disappeared. The loss of protrusions created an excess plasma membrane area, which was transformed into chains of pearls sticking out of the area of the plasma membrane that enveloped the rounded cell body (Fig. 1 *B*).

At the beginning of latA action, actin remained transiently clustered at the plasma membrane, primarily in contact with clathrin-coated pits (2). After 15 min the actin was depolymerized to an extent that in most cells no structures of microscopic size remained recognizable with LimEΔ-GFP (Movie S1 in the Supporting Material). However, with GFP-coronin, which associates with depolymerizing actin structures (22,30) the pearls were intensely labeled (Fig. 1 *C*), suggesting that slowly dissociating complexes of actin filaments were still present. To visualize these complexes, we subjected latA-treated cells to cryo-ET. In a subset of pearls, bundles of straight or slightly bent actin filaments were detectable, which were too short for deforming the pearls (Fig. 1, *D* and *E*, and Movie S2).

Because pearling is a phenomenon observed in pure lipid membranes, we explored the possibility that the pearling of membrane tubes in *Dictyostelium* cells is caused by unmixing of the lipid phase from the protein-containing plasma membrane. GFP-PLCδ1 was expressed in the cells, which recognizes phosphatidylinositol- (4,5) bisphosphate (PIP2) (31), and cells were labeled with FITC-concanavalin A, which preferentially binds to glycosyl residues that are N-linked to membrane proteins of *Dictyostelium* cells (32). These labels did not distinguish the membrane of the pearls from the plasma membrane on the cell body indicating that, together with lipids, membrane proteins enter the pearling membrane protrusions (Fig. 2, *A* and *B*, and Movie S3).

Pearling by membrane protrusion or retraction of the cell body

Two modes of transformation of the plasma membrane into pearls were observed in cells adhering to a glass surface: 1), protrusion of chains of pearls, some of them in contact with the substrate surface, other ones freely extending into the fluid medium as shown by their Brownian movement (Fig. 2 *C* and Movie S4); 2), retraction of the cell from the substrate, leaving substrate-attached pearls behind (Fig. 2 *D* and Movie S5). The different modes of pearl formation were reflected in highly variable pearl sizes, ranging from diameters of 0.22 μm, as revealed by cryo-ET, to 3 μm. We obtained also extensive pearling by combining 10 μM lat A with 10 μM cytochalasin A, a blocker of the plus ends of actin filaments, indicating that even efficient depolymerization of actin does not prevent the membrane from pearling. Combination of the two drugs resulted again in pearls-on-a-string and variable

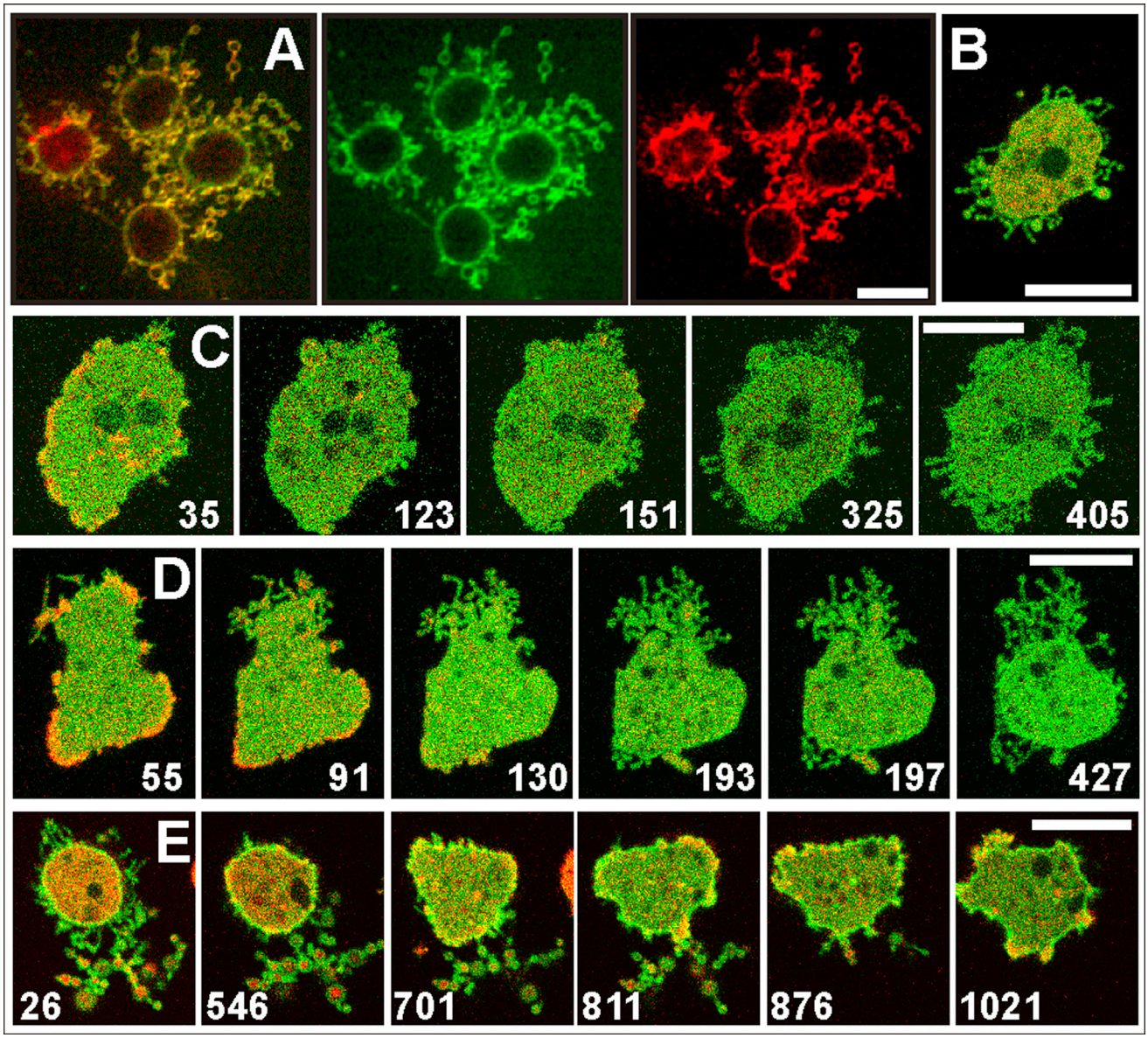

FIGURE 2 Pearling membranes labeled with concanavalin A or PLCδ1. (*A*) Cells labeled with FITC–concanavalin A (*green*), a lectin binding preferentially to α-mannosyl residues on N-glycosylated proteins, and counterstained with Alexa Fluor 568 succinimidyl ester, a cell surface marker (*red*). The three panels display merged images (*left*), the concanavalin A label (*middle*), and the cell-surface label (*right*). (*B*) Cell expressing mRFP- LimEΔ (*red*) and GFP-PLCδ1, which recognizes PI(4,5)P_2 (*green*). PI(4,5)P_2 is localized to the membrane of the pearls as well as to the plasma membrane enveloping the cell body. (*C*) Pearl formation by protrusion of the cell surface. (*D*) Pearl formation by retraction of the cell. In both (*C*) and (*D*) pearl formation begins at a late stage of actin depolymerization. (*E*) Withdrawal of pearls during the repolymerization of actin. Cells in (*C–E*) were labeled similar to the cell in (*B*). Patches of PLCδ1 indicate local enrichment of PIP2 under conditions of intense clathrin-dependent endocytosis (2), in accord with a role of PIP2 in membrane invagination (69). Numbers indicate seconds after the addition (*C* and *D*) or the removal of 5 μM latA (*E*). Bars, 10 μm. The time series corresponding to (*B–E*) are displayed in Movies S3–S5, S7.

pearl sizes (Movie S6), suggesting that incomplete or delayed actin depolymerization is not responsible for the variability.

To inquire whether pearling membranes are still in a native state, we explored the reversibility of pearling after latA removal during the recovery of normal cell motility. Fig. 2 *E* and Movie S7 show that pearled protrusions of the cells can be pulled back and reintegrated into the plasma membrane. Only a few protrusions, in particular those strongly adhering to the substrate, became disconnected.

Reversible compartmentation of the cell

Reintegration of the membrane of pearls into the plasma membrane suggests continuity of the pearl membrane with

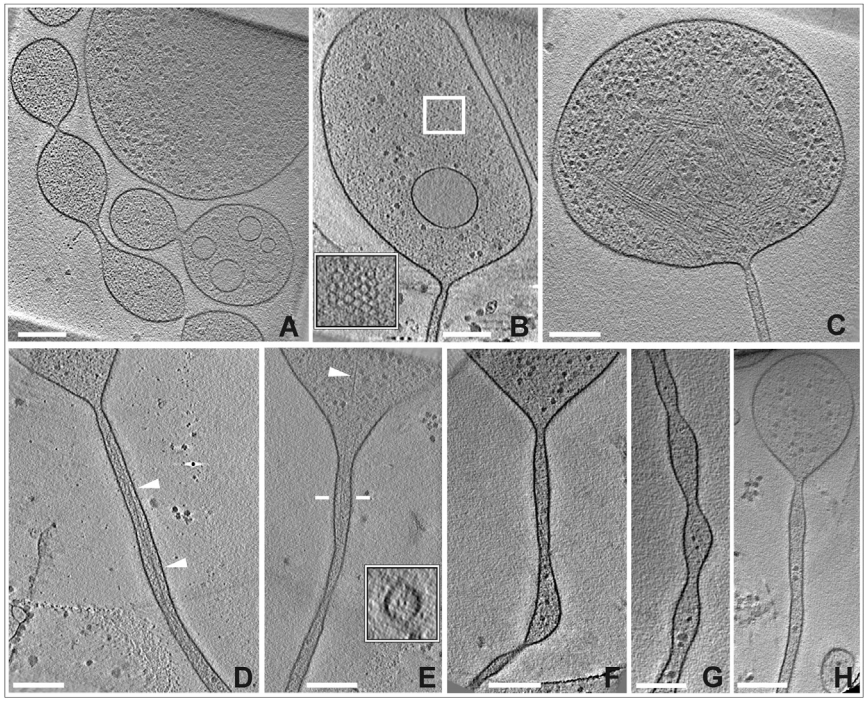

FIGURE 3 Tomograms of pearls and tubes. Pearling was induced by incubating cells with either 5 μM (*A–F*) or 30 μM (*G* and *H*) latA. (*A*) Pearls connected to each other or separated by short tubes. (*B* and *C*) Pearls extending into long tubes, showing constrictions at the pearl-tube interface. The inset in (*B*) shows a clathrin-coated pit visible in another slice of the tomogram. In (*C*) bundled actin filaments are retained, similar to Fig. 1 *D*. (*D–H*) Gallery of long nanotubes, two with actin filaments (*D* and *E*) and three with no detectable filaments (*F–H*). The arrowheads in (*D*) and (*E*) point to long filaments; in *E* the filament extends from the pearl into the upper part of the tube. The inset in (*E*) shows a cross section through the tube at the position indicated by bars, displaying a bundle of two filaments inside. A bent tube is shown in (*F*), and a tube with periodic variations of diameter in (*G*). All images show slices through tomograms. A 3D reconstruction of (*C*) is displayed in Movie S8 together with the 3D segmentation of the filaments and the membrane. Bars, 200 nm; the insets in (*B*) and (*E*) are twofold magnified relative to the main figure.

that enveloping the cell body. The question of whether the contents of the pearls is connected with the cytoplasm was addressed using FRAP in cells that expressed free GFP, which is purely cytosolic and has a diffusion constant D = 42 $\mu m^2 \times s^{-1}$ in *Dictyostelium* cells in the absence of filamentous actin (33). FRAP of GFP in the cell body was accordingly fast (Fig. S1 *A*). When pearls were bleached, recovery was slow, incomplete, or absent. No recovery meant that GFP molecules with a size of 3–4 nm were prevented from diffusion through the tubes that separated a pearl from other pearls or from the cell body. Incomplete recovery indicated no connection to the GFP reservoir of the cell body (Fig. S1 *B*).

Pearl and tube structures revealed by cryo-ET

To determine the diameter of the tubes connecting the pearls and to examine whether these tubes can be formed in the absence of microfilaments extending along their axis, we have applied cryo-ET on cells treated with either 5 or 30 μM latA. Cells were incubated with the drug on a carbon film and vitrified after ~15 min. In one experiment the cells were resuspended by pipetting, to disconnect the tubes from any support that could exert tension, before the cells were allowed to settle on the film.

The pearls were directly connected to each other (Fig. 3 *A*) or separated by tubes (Fig. 3, *B–H*). Sometimes these tubes were branched, or bent as shown in Fig. 3 *F*; this argues against forces acting in stretching the tubes between two points along their surface that might be fixed on the carbon film. Periodic variations of the tube diameter, as displayed in Fig. 3 *G*, suggest an incomplete stage of tube-pearl differentiation.

The tubes and pearls were unilamellar; the pearls commonly containing vesicles of variable sizes (Fig. 3, *A* and *B*), and also clathrin-coated pits (Fig. 3 *B*). The cytoplasm entrapped in the pearls was rich in ribosomes and also populated with larger particles of ~50 nm diameter (Fig. 3 *C*). The presence of such particles in tubes (Fig. 3 *G*) might be responsible for narrowing the space for diffusion of GFP molecules, as shown in Fig. S1.

In cells treated with 5 μM latA, a fraction of the pearls and of the tubes connecting them still contained microfilaments (Fig. 1, *D* and *E*, and Fig. 3, *C–E*).

Other pearls and tubes formed at 5 μM latA appeared to be free of microfilaments (Fig. 3 *F*). To substantiate the independence of pearl formation from an actin support, we applied 30 μM latA, which rapidly and efficiently eliminated any actin clusters but did not prevent pearling. At this very high concentration, chains of pearls were formed during the disappearance of actin structures, either on the substrate or protruding freely into the extracellular space (Movie S9). In the tomograms, we no longer detected microfilaments in the tubes or pearls (Fig. 3, *G* and *H*). This means, the tubes were free of filaments that could support myosins in applying tension for pulling out membrane tubes.

The diameters of the microfilament-depleted tubes varied not only from one tube to the other but also along a single tube, most evidently in tubes with an oscillating diameter as shown in Fig. 3 *G*. The diameters of uniform tubes that were depleted of actin ranged from 38 to 46 nm, measured

as the distance between the middle of the electron-dense membranes. Often a constriction reducing the tube diameter to ~29 nm was observed close to the pearl-tube interface (Fig. 3, *B*, *C*, and *H*). This constriction is in accord with theoretical predictions (34) and observations on tubes pulled out of giant lipid vesicles (35).

Pearl formation is microtubule independent

The possibility that chains of pearls are protruded or retracted by the polymerization/depolymerization of microtubules or by forces applied by microtubule-dependent motors, was examined by the labeling of microtubules using GFP-α-tubulin (21) and by depolymerizing the microtubules using nocodazole. In the absence of the drug, we never saw a microtubule form along the axis of an emerging chain of pearls (Fig. S2 *A*), nor have we seen microtubules enter these chains during retraction of the pearls into the cell body (Fig. S2 *D*).

In cells incubated with nocodazole, the microtubule length was strongly reduced such that their ends could no longer touch the plasma membrane from where pearls are emanating. Nevertheless, pearls were formed in the presence of latA (Fig. S2, *B* and *C*, and Movie S10) and were retracted after its removal (Movie S11). An exceptional mode of recovery is shown in Fig. S2 *E*, where cytoplasm filled the lumen of a chain of pearls, in that way opening the constrictions that separate the pearls.

Formation and retraction of pearls does not require myosin-II and is thus distinguished from blebbing

Myosin-II is the motor protein that in cooperation with filamentous actin is responsible for tail contraction in migrating *Dictyostelium* cells. Myosin-II generates also the rigor resulting in the contraction of cells that are depleted of ATP (36). The increase of membrane tension caused by the depletion of ATP in cells of *D. discoideum* results in local disruption of the actin cortex and blebbing of the cell surface. Although a thin layer of filamentous actin covers the membrane of the blebs, the majority of actin filaments are clustered in the interior of the cell together with myosin-II and certain actin-binding proteins (37).

Wild-type (WT) and mutant cells that lack myosin-II heavy chains (myo-II HC-null cells) were exposed to 2,4-dinitrophenol. This uncoupler of oxidative phosphorylation is known to decrease cellular ATP to ~10% of its normal level. Under these conditions, which reduce the resistance of the actin cortex, WT cells are induced to bleb within 3 min (37). The cells stay alive and return to normal shape and motility as soon as the uncoupler is removed. Fig. 4, *A–D*, shows that myosin-II is required for cell-surface blebbing under the conditions of ATP depletion: in contrast to WT cells, the myo-II HC-null cells did not bleb. They changed their shape only slowly by rounding up (Movie S12).

To distinguish the mechanism of pearling from that of blebbing, we treated myo-II HC-null cells with latA. These mutant cells showed intense pearling (Fig. 4, *E* and *F*, and Movie S13). The formation of pearls in the mutant cells resembled that of WT cells (compare in Fig. 2 *D* and Fig. 4 *E* the pearling by retraction of the cell body). During recovery of the mutant cells, the pearls are efficiently withdrawn; in the example shown in Fig. 4 *G*, the pearling stage is followed by the propagation of an actin wave (Movie S14), similar to wave formation in WT cells (2).

Spreading of pearling cells on a glass surface

The spreading of cells on an adhesive surface involves shape changes, phase transitions, as well as regulation of the surface area and membrane tension. These regulations are mediated by the actin system in *Dictyostelium* (38) as in mammalian cells (39–41). Nevertheless, *Dictyostelium* cells can spread even in the pearling state. LatA-treated *Dictyostelium* cells produce pearling tubes also in suspension. Because these cells will adhere to a glass surface not only with the compact surface of their body but also with the pearling protrusions, we have monitored the spreading behavior of cells in the presence of latA. As shown in Fig. 5 and Movie S15, a latA-treated cell can turn from initial substrate contact, made by the tips of pearling membrane tubes, to expansion of the cell body on the substrate. Subsequently, contact with the substrate induced new tubes, followed by pearling as displayed in Fig. 6 and Movie S16. These time series show that cells devoid of an actin cortex can spread on an adhesive surface, and they do so by the formation of pearling tubes.

DISCUSSION

Reversible pearling of plasma membranes lacking an actin support

The membrane pearling studied here is an autonomous process that occurs in live cells when support by the cortical actin network is lacking. Sizes of the pearls ranged in our experiments from 0.2 to 3 μm diameter, as seen in Fig. 6 *B* and Movie S16, and thin tubes connecting the pearls had a diameter of ~40 nm. Microtubules are not involved in protrusion or retraction of the chains of pearls formed upon the depolymerization of actin, and the pressure-generating activity of myosin-II is dispensable. Pearls can emanate from the free cell surface, which means that tension produced by adhesion to the substrate is not required, although the pearls may adhere to a glass surface if they come into contact with it. To find out whether the contents of the pearls is continuous with, or separated from, the

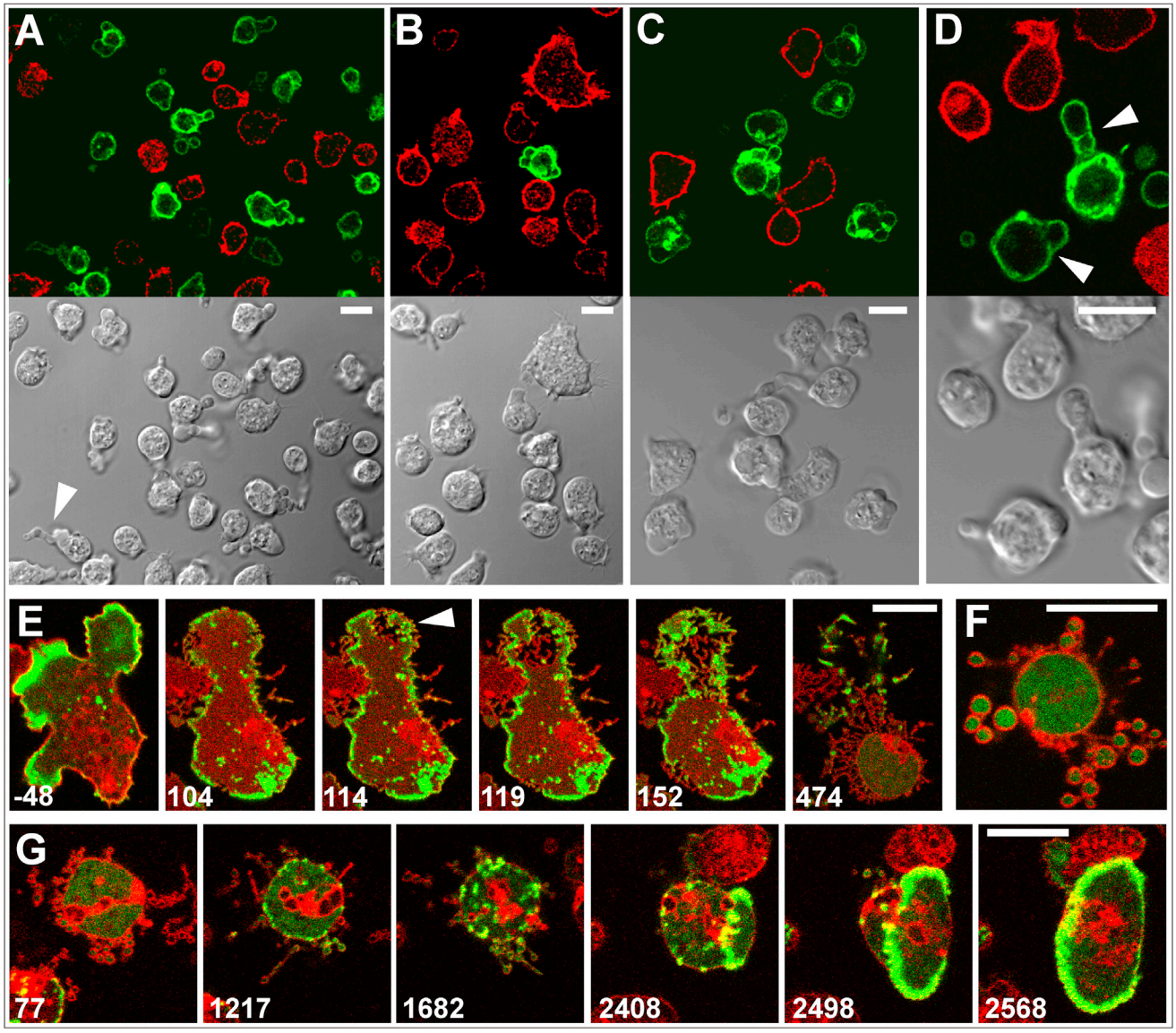

FIGURE 4 Pearling distinguished from blebbing by its independence of myosin-II. (*A–D*) Blebbing induced in WT cells by the decline of cellular ATP. WT cells expressing GFP- LimEΔ (*green*) mixed with myo-II HC-null cells expressing mRFP-LimEΔ (*red*) were exposed to 50 μM or, in (*C*), to 100 μM 2,4-dinitrophenol. The bottom panels show differential interference contrast bright-field images, the top panels confocal fluorescence scans. In the overview of (*A*) a cell forming a chain of blebs is indicated by an arrowhead. In (*B*) the large mutant cell on top displays filopodia, whereas the WT cell below forms multiple blebs. In WT cells of (*C*) a thin actin layer persists at the membrane of the blebs, whereas the majority of actin is separately clustered. In the optical sections of (*D*) septa of actin are recognizable through which blebs are broken (*arrowheads*). A time series corresponding to (*A–D*) is shown in Movie S12. (*E–G*) Pearling in myo-II HC-null cells. These mutant cells expressed LimEΔ- GFP to label filamentous actin (*green*); they were stained with FM4-64 (*red*) and incubated in 5 μM latA. The arrowhead at the large cell of (*E*) points to an area where transformation of the membrane into pearls begins. A mutant cell forming large pearls is shown in (*F*), and the withdrawal of pearls in a mutant cell in (*G*). Here, a propagating actin wave was formed at the final stage of reintegration of the pearled membrane into the cell surface. Actin waves are typical of an intermediate stage of recovery from actin depolymerization (2). Numbers in (*E*) and (*F*) indicate seconds before or after the addition of latA, in (*G*) after its removal. Bars, 10 μm. Time series corresponding to (*E*) and (*G*) are shown in Movie S13 and Movie S14.

cytoplasm of the cell, we have applied FRAP to cells expressing free GFP. The tubes, which separate each pearl from its neighbors in a chain, together with the particles within these tubes, largely reduce or completely abolish the exchange of proteins between the pearls and between the pearls and the cell body. Nevertheless, the membranes of the pearls can be reintegrated into the envelope of a cell during recovery of actin polymerization.

The fact that at a concentration of 5 μM, latA did not completely depolymerize the actin, enabled us to reconstruct tomograms of the most resistant actin assemblies. These consisted of microfilament bundles of variable

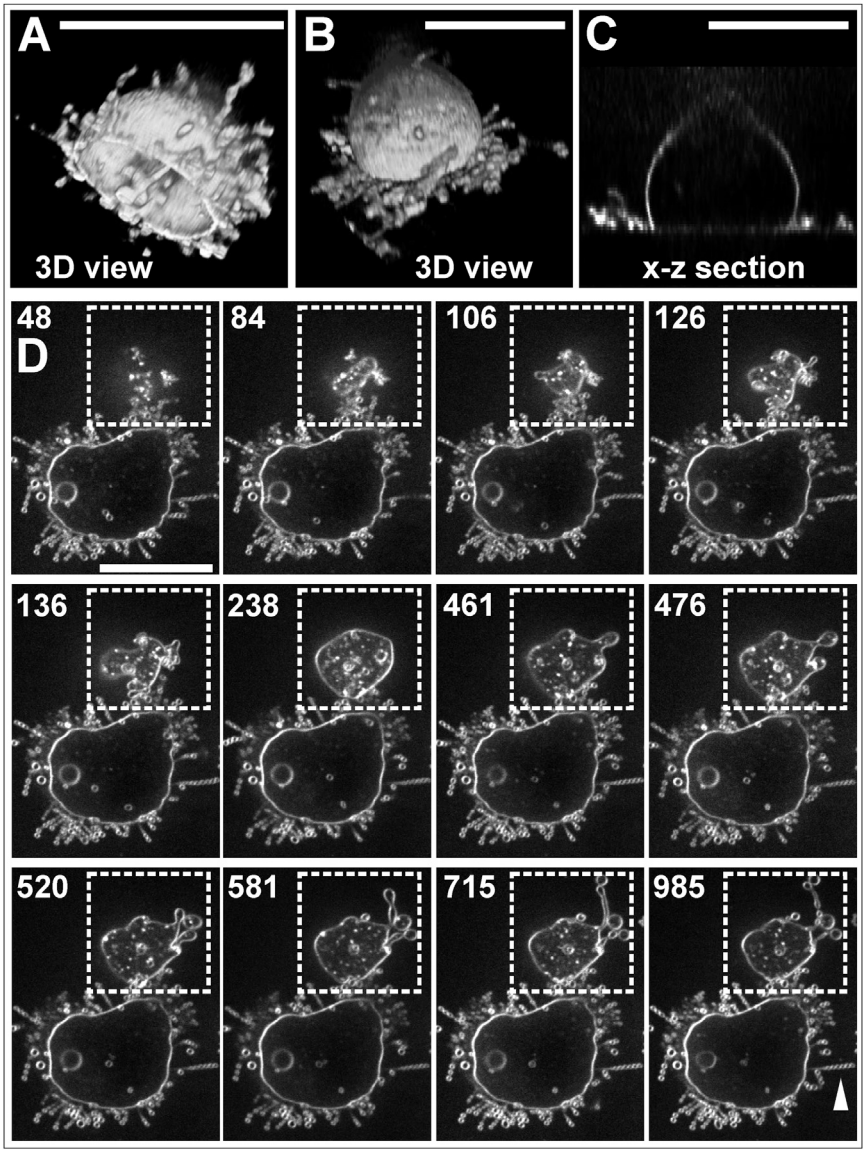

FIGURE 5 Spreading of cells preincubated with 5 μM latA before subjecting them onto a coverslip. Membranes were stained using FM4-64. (*A–C*) Shape of two cells preincubated with latA and attached for 2 min (*A*) or 50 min (*B* and *C*) to a glass surface. In the 3D reconstruction of the cell shown in (*A*), membrane tubules are primarily pointing into the fluid space. The 3D reconstruction in (*B*) shows many pearled tubes spread along the substrate surface, the cross section in (*C*) the cell body to rise from the substrate at an angle of ~73°. (D) Stages of spreading on a strongly adhesive fluoralkane-coated surface. The framed upper cell proceeds to spread, whereas the bottom cell is already in a stable spreading state. The arrowhead points to a long chain of pearls. Numbers indicate seconds after the first contact of the upper cell with the glass surface. The full time series corresponding to this figure is presented in Movie S15. Bar, 10 μm.

orientation, which were of limited length and did no longer deform the pearls (Fig. 1, *D* and *E*, Fig. 3 *C*, Movie S2, and Movie S8).

Membrane pearling is distinct from myosin-II-based blebbing and from microtubule-supported tubulation

The pearling phenomenon is distinct from membrane blebbing caused by an increase in rigor, which leads to local rupture of the actin cortex followed by the repolymerization of actin beneath the membrane of a bleb (42). An increase in rigor is observed in *Dictyostelium* cells when the synthesis of ATP is inhibited by azide (36). In a reversible manner, the blebbing is induced by 2,4-dinitrophenol, a membrane permeable uncoupler of oxidative phosphorylation (37). The distinguishing feature of blebbing is that the force is generated by the contractile activity of myosin-II, such that myosin-II null mutant cells of *D. discoideum* (Fig. 4, *A–D*), or M2 macrophages treated with the myosin-II ATPase inhibitor blebbistatin (43,44) do not bleb. In contrast, pearling tubes are still formed in myosin-II null mutants (Fig. 4, *E–G*).

We note that myosin-II null cells have been reported to bleb if they are stimulated with a high concentration of cyclic AMP (45). From blebbing under our conditions this chemoattractant-induced blebbing is distinguished by the formation of rounded protrusions that are filled with filamentous actin, as indicated by phalloidin labeling. Obviously, this type of blebbing does not require an increase in tension that is generated by myosin-II.

Microtubules can support the tubulation of membranes in two ways. First, phospholipid vesicles are deformed from within by the polymerization of microtubules (46). Second, lipid membranes can be pulled into nanotubes by the walking of microtubule-based motors along their outer

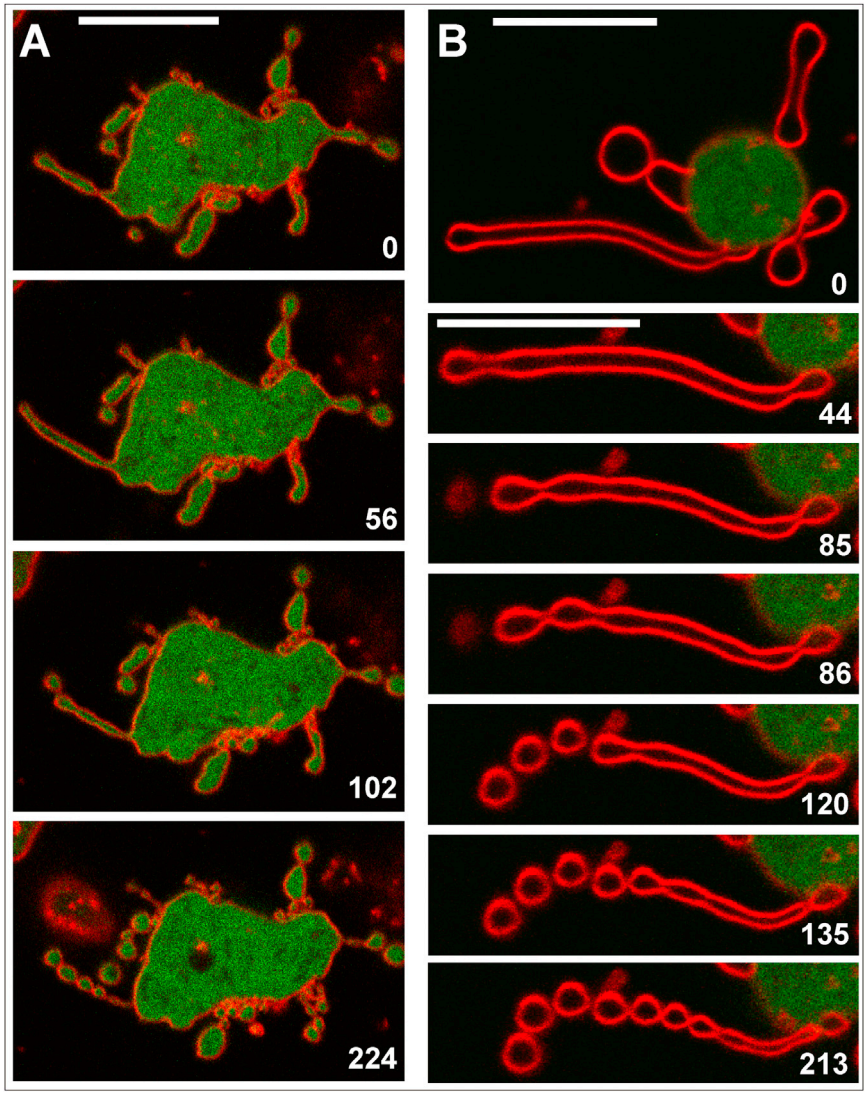

FIGURE 6 Transformation of tubes into pearls in spreading cells. The cells expressing LimEΔ-GFP (*green*) were incubated for 30 min with latA in gently shaken suspension before they were transferred onto a glass surface and FM4-64 (*red*) was added. At that time no filamentous actin structures were detectable by the LimEΔ-GFP label. (*A*) A spreading cell protruding multiple tubes, the left one is subdivided into five pearls. (*B*) A tube protruded by a spreading cell, which is from top to bottom progressively organized into pearls. Numbers indicate seconds after the first frame in each panel. Bars, 10 μm. The pearling sequence shown in (*B*) is displayed in Movie S16.

surface. In that way, membranes of the endoplasmic reticulum are drawn in vivo into tubes (47), and in vitro the lipid membranes of GUVs are pulled along microtubules by kinesins (12). The pearling membrane tubes studied by us in live cells were not populated with microtubules, and these membrane tubes can be formed and retracted after microtubule depolymerization (Fig. S2). We conclude that formation and pearling of the membrane tubes in *Dictyostelium* cells are not based on microtubule-dependent force generation. In tubes formed at a latA concentration as high as 30 μM, no actin filaments were detected by cryo-ET, excluding the possibility that any myosin motors generate the force for tubulation.

Pearling tubes are a favored state of unsupported plasma membranes

In *Dictyostelium* cells depleted of a submembraneous actin layer, the plasma membrane is divided into two distinct portions, the envelope of the cell body and the excess membrane area. The cell body is rounded; when attached to glass its surface arises from the substrate at a large angle of ~73° (Fig. 5 *C*). This shape suggests that the smooth membrane closely surrounding the cell body is under tension, and the size of its area is kept at a minimum, whereas the excess plasma membrane not supported by an actin layer has a high propensity of organizing into tubes that undergo a transition into chains of pearls.

A phenomenon that may be compared with tube formation in actin-depleted cells has been discovered in giant lipid vesicles that encapsulate two aqueous phases, dextran and polyethylene glycol (PEG) (48). Upon deflation of these vesicles, excess membrane is generated and transformed into nanotubes that extend from the vesicle surface into the interior of the PEG phase. This shape transformation is reversible, as the increase of membrane tension results in retraction of the nanotubes back into the surface membrane of the vesicle. Theoretical analysis revealed that the

conversion of excess membrane into nanotubes is driven by the spontaneous curvature that the membrane assumes in contact with the internal PEG phase. By the same argument, the pearled membrane tubes that are reversibly protruded from the surface of *Dictyostelium* cells into the extracellular space might represent an energetically favored state of the unsupported plasma membrane of a live cell. In this case, one may assume that the membrane is transformed into pearled tubes until this transformation is counteracted by the increasing membrane tension on the surface of the cell body. This notion is underscored by the fact that pearling is reversible. Reversibility indicates that the pearled portion of the membrane is continuous with the fraction of the plasma membrane that envelops the rounded cell body.

Pearl dynamics in spreading cells

When cells attached to a glass surface are incubated with latA, tube formation and pearling will end up in a stationary state of pearls that are either free or attached to the surface, as shown in Fig. 1 *B* and Movie S1. When cells are incubated in suspension, they also form tubes and pearls. The nonrequirement of cell-substrate adhesion for pearl formation is disclosed by imaging cells on a nonadhesive polyethylene glycol-coated surface that are incubated in suspension with 5 μM latA (data not shown). However, the stationary state is disturbed if the suspended cells are brought into contact with an adhesive substrate. Spreading of these cells implies the protrusion of new tubes and their transformation into chains of pearls (Fig. 5 *D* and Fig. 6). This reorganization indicates that, even after long incubation with latA, the states of the membrane are still convertible and adhesion energy is capable of shifting the state toward pearling.

Mechanisms of membrane pearling

The behavior of the complex plasma membrane of living cells may be compared with that of model lipid membranes. If local forces are acting on a giant unilamellar phospholipid vesicle (GUV), tubes with a radius in the tens of nanometer range can be pulled out of the vesicle (9). In membrane tubes that are stretched using a laser trap, a Rayleigh-like instability can be elicited, resulting in the generation of pearls on a string that can travel along the thin tube connecting them (16). When the tension is released by turning off the tweezers that stretch the tube, the pearling state relaxes into a straight cylinder.

Conversion of a tube into a chain of pearls may also be caused by an increase in its volume due to high osmotic pressure (19). In the case of pearling tubes that exchange GFP molecules with the cell body (Fig. S1 *B*) this is unlikely the mechanism to work because the pressure would be released from the lumen of the tubes into the cell body where the contractile vacuoles serve as osmoregulators.

The study of membrane pearling in live cells has been pioneered by Bar-Ziv et al. (4). These authors discovered that in membrane tubes of SVT2 cells, pearling resulted from the competition of surface tension with curvature energy. The tension was supplied by local attachment of the tubes to a solid substrate. As the pearling in lipid vesicles, that of the plasma membrane was interpreted as a Rayleigh-like instability. A distinguishing feature of the pearling studied by us is its independence of an external source of tension, as evidenced by the formation of pearls on the free portion of the cell surface. Whereas the pearling in (4) required actin to be only partially depolymerized, that in *Dictyostelium* cells occurred even after efficient depolymerization (Fig. 3, *G* and *H*, Movie S6, and Movie S9). In contrast to the pearls in stretched lipid vesicles, those in *Dictyostelium* cells assume a fixed position along the tubes even if they are not attached to a substrate (as seen in Movies S3, S4, and S9).

An alternative mechanism underlying shape changes in vesicles is the coupling of membrane curvature and local composition in two- or multicomponent systems (49,50), which can lead to the formation of a bud separated from the vesicle by a neck at a site where two domains meet (51). The local curvature of membranes can be determined by their protein or lipid composition. The shape of vesicles composed of a ternary mixture of two phospholipids and cholesterol is determined by several parameters. 1), Line tension drives the boundary between a L_0 and a L_d domain to a minimum radius, resulting in a constriction along the boundary (10). 2), In the L_d phase, lipids have a higher diffusion coefficient (52) and bending is facilitated (10). Because the L_0 phase is more rigid, it is excluded from membrane tubes that are pulled out of GUVs (53). Accordingly, the more flexible L_d phase will sort into regions of higher curvature than the L_0 phase with short-range order (54). 3), If the separated domains differ in the geometry of lipid molecules, they tend to assume concave or convex curvature (55). Cone-shaped lipids such as double-chain phospholipids will prefer concave membrane areas as opposed to inverted-cone-shaped lipids such as saturated lysophospholipids, which prefer convex areas. This coupling of curvature to lipid segregation needs to be specified because experimental data revealed that individual conical or inverted-cone-shaped phospholipid molecules are too small to show more than a weak curvature preference (56). Larger lipids, such as gangliosides, may have stronger curvature preferences. However, even small phospholipids may be strongly coupled to curvature if they are clustered.

Examples for proteins that force membranes to bend are dynamins and BAR or I-BAR domain-containing proteins. Dynamins bind to PIP2-supplemented nanotubes with a preferred radius of 11 nm, and stabilize these tubes by polymerizing on their outer surface (57). F-BAR or I-BAR proteins accumulate at the cytoplasmic face of convex or concave membrane regions and force the membranes to

bend (58). The F-BAR proteins polymerize and form lattices on the outer surface of membrane tubes (59).

Dictyostelium cells contain two dynamins, A and B, which participate in endocytic trafficking (60,61). One I-BAR protein has been identified in *D. discoideum*, which accumulates at clathrin-coated structures immediately before endocytosis (62) and at the neck region of particles that are being phagocytized (22). Two proteins containing an F-BAR domain are involved in transforming the membrane of the contractile vacuole into tubules (63).

A protein that shapes membrane tubes by associating with their inner, i.e., cytoplasmic face, would be needed to sculpt the tubes in pearling *Dictyostelium* cells. We cannot strictly rule out the presence of such a protein. However, our tomograms provide no evidence for a regular lattice of proteins on the tubular membrane. Therefore, we consider the sorting out of cone-shaped and inverse-cone-shaped lipids as a reasonable mechanism for the pearl-tube differentiation of the plasma membrane in the absence of an actin network. In the complex membranes of eukaryotic cells that contain sterols (primarily Δ^{22}-stigmasten-3β-ol in the case of *Dictyostelium* cells (64,65)), such coupling is likely to be effective and responsible for the periodicity of convex and concave areas in the pearling state.

The separation of L_d and L_o phases in membranes requires that temperatures are below a demixing point (66). The fact that the optimal temperature for the growth and development of *Dictyostelium* cells is ~23°C rather than 37°C as for mammalian cells, is supposed to favor phase segregation in the membranes under natural living conditions.

How does the actin network prevent pearling?

Because the plasma membrane of a live cell has a complex composition of lipids and integral or associated proteins, it is reasonable to assume that lipids and proteins known to enforce membrane bending play a role in pearling. Actin networks may hinder membrane components from sorting by two mechanisms that are not mutually exclusive. 1), Cross-linked actin filaments and bundles form a fence that restricts fast diffusion in the membrane to small meshes, with a low probability of hopping over the barriers (67). Experimental analysis of a minimal membrane-cortex model and Monte Carlo simulations revealed partial confinement of lipid and protein within actin meshes, with a stronger effect on the larger protein (68). 2), The submembraneous actin layer increases the bending stiffness of a composite membrane, in that way cutting off the positive feedback of curvature generation and protein or lipid sorting. In the absence of a supporting actin network, the unmixing of cone-shaped and inverted-cone-shaped lipids will be enhanced by the positive feedback: stochastic clustering of one or the other type of lipid should cause slight local bending of the membrane, which will favor the accumulation of more lipids of the same class and in turn enhance the bending. According to this hypothesis, the feedback circuit would be cut off and consequently unmixing and pearling prevented if the membrane bending is suppressed by an actin support.

In summary, our data are consistent with a function of the membrane-associated actin network in cutting off the positive feedback of lipid (and probably protein) sorting and membrane curvature. This feedback may, in the absence of an actin network, enhance the sorting of lipids (and proteins) that create a certain membrane curvature and favor this curvature for accumulating. Experiments that combine model lipid membranes with in vitro generated actin networks of defined mechanical properties would be needed to analyze the mechanisms by which the cortical actin layer prevents membrane pearling.

SUPPORTING MATERIAL

Two figures and sixteen movies are available at http://www.biophysj.org/biophysj/supplemental/S0006-3495(14)00134-9.

We thank Wolfgang Baumeister, MPI for Biochemistry, for his support and Harald Engelhardt for discussions on Cryo-ET, Britta Schroth-Diez, MPI-CBG, for cooperation in FRAP experiments and TIRF imaging.

D.H. is grateful to Joachim Spatz, MPI for Intelligent Systems, for supporting her and also acknowledges funding by the Fraunhofer Society within the "Attract" scheme. We acknowledge equipment and technical support of the Nikon Imaging Center at the University of Heidelberg, and thank the Max Planck Society for support to G.G.

REFERENCES

1. Heuser, J., Q. Zhu, and M. Clarke. 1993. Proton pumps populate the contractile vacuoles of *Dictyostelium* amoebae. *J. Cell Biol.* 121: 1311–1327.
2. Schroth-Diez, B., S. Gerwig, …, G. Gerisch. 2009. Propagating waves separate two states of actin organization in living cells. *HFSP J.* 3: 412–427.
3. Gerisch, G., T. Bretschneider, …, K. Anderson. 2004. Mobile actin clusters and traveling waves in cells recovering from actin depolymerization. *Biophys. J.* 87:3493–3503.
4. Bar-Ziv, R., T. Tlusty, …, A. Bershadsky. 1999. Pearling in cells: a clue to understanding cell shape. *Proc. Natl. Acad. Sci. USA.* 96:10140–10145.
5. Sackmann, E. 1994. The seventh Datta Lecture. Membrane bending energy concept of vesicle- and cell-shapes and shape-transitions. *FEBS Lett.* 346:3–16.
6. Baumgart, T., A. T. Hammond, …, W. W. Webb. 2007. Large-scale fluid/fluid phase separation of proteins and lipids in giant plasma membrane vesicles. *Proc. Natl. Acad. Sci. USA.* 104:3165–3170.
7. Veatch, S. L., P. Cicuta, …, B. Baird. 2008. Critical fluctuations in plasma membrane vesicles. *ACS Chem. Biol.* 3:287–293.
8. Seul, M., and D. Andelman. 1995. Domain shapes and patterns: the phenomenology of modulated phases. *Science.* 267:476–483.
9. Sens, P., and M. S. Turner. 2011. Microphase separation in nonequilibrium biomembranes. *Phys. Rev. Lett.* 106:238101.
10. Baumgart, T., S. T. Hess, and W. W. Webb. 2003. Imaging coexisting fluid domains in biomembrane models coupling curvature and line tension. *Nature.* 425:821–824.

11. Heinrich, V., B. Božič, …, B. Žekš. 1999. Vesicle deformation by an axial load: from elongated shapes to tethered vesicles. *Biophys. J.* 76:2056–2071.
12. Roux, A., G. Cappello, …, P. Bassereau. 2002. A minimal system allowing tubulation with molecular motors pulling on giant liposomes. *Proc. Natl. Acad. Sci. USA.* 99:5394–5399.
13. Koster, G., M. VanDuijn, …, M. Dogterom. 2003. Membrane tube formation from giant vesicles by dynamic association of motor proteins. *Proc. Natl. Acad. Sci. USA.* 100:15583–15588.
14. Leduc, C., O. Campas, …, P. Bassereau. 2010. Mechanism of membrane nanotube formation by molecular motors. *Biochim. Biophys. Acta.* 1798:1418–1426.
15. Shaklee, P. M., T. Idema, …, M. Dogterom. 2008. Bidirectional membrane tube dynamics driven by nonprocessive motors. *Proc. Natl. Acad. Sci. USA.* 105:7993–7997.
16. Bar-Ziv, R., and E. Moses. 1994. Instability and "pearling" states produced in tubular membranes by competition of curvature and tension. *Phys. Rev. Lett.* 73:1392–1395.
17. Zhu, T. F., K. Adamala, …, J. W. Szostak. 2012. Photochemically driven redox chemistry induces protocell membrane pearling and division. *Proc. Natl. Acad. Sci. USA.* 109:9828–9832.
18. Yu, Y., and S. Granick. 2009. Pearling of lipid vesicles induced by nanoparticles. *J. Am. Chem. Soc.* 131:14158–14159.
19. Zeitz, M., and P. Sens. 2012. Reversibility of red blood cell deformation. *Phys. Rev. E Stat. Nonlin. Soft Matter Phys.* 85:051904.
20. Bretschneider, T., S. Diez, …, G. Gerisch. 2004. Dynamic actin patterns and Arp2/3 assembly at the substrate-attached surface of motile cells. *Curr. Biol.* 14:1–10.
21. Neujahr, R., R. Albrecht, …, G. Gerisch. 1998. Microtubule-mediated centrosome motility and the positioning of cleavage furrows in multinucleate myosin II-null cells. *J. Cell Sci.* 111:1227–1240.
22. Clarke, M., U. Engel, …, G. Gerisch. 2010. Curvature recognition and force generation in phagocytosis. *BMC Biol.* 8:154–176.
23. Manstein, D. J., M. A. Titus, …, J. A. Spudich. 1989. Gene replacement in *Dictyostelium*: generation of myosin null mutants. *EMBO J.* 8: 923–932.
24. Fischer, M., I. Haase, …, A. Müller-Taubenberger. 2004. A brilliant monomeric red fluorescent protein to visualize cytoskeleton dynamics in *Dictyostelium*. *FEBS Lett.* 577:227–232.
25. Mastronarde, D. N. 2005. Automated electron microscope tomography using robust prediction of specimen movements. *J. Struct. Biol.* 152:36–51.
26. Kremer, J. R., D. N. Mastronarde, and J. R. McIntosh. 1996. Computer visualization of three-dimensional image data using IMOD. *J. Struct. Biol.* 116:71–76.
27. Stalling, D., M. Westerhoff, and H.-C. Hege. 2005. Amira: a highly interactive system for visual data analysis. *In* Visualization Handbook. D. H. Charles and R. J. Chris, editors. Butterworth-Heinemann, Burlington, MA, p. 749.
28. Rigort, A., D. Günther, …, H.-C. Hege. 2012. Automated segmentation of electron tomograms for a quantitative description of actin filament networks. *J. Struct. Biol.* 177:135–144.
29. Clarke, M., J. Köhler, …, G. Gerisch. 2002. Endosome fusion and microtubule-based dynamics in the early endocytic pathway of *dictyostelium*. *Traffic.* 3:791–800.
30. Ishikawa-Ankerhold, H. C., G. Gerisch, and A. Müller-Taubenberger. 2010. Genetic evidence for concerted control of actin dynamics in cytokinesis, endocytic traffic, and cell motility by coronin and Aip1. *Cytoskeleton (Hoboken).* 67:442–455.
31. Stauffer, T. P., S. Ahn, and T. Meyer. 1998. Receptor-induced transient reduction in plasma membrane PtdIns(4,5)P2 concentration monitored in living cells. *Curr. Biol.* 8:343–346.
32. Hohmann, H. P., S. Bozzaro, …, G. Gerisch. 1987. Two-step glycosylation of the contact site A protein of *Dictyostelium discoideum* and transport of an incompletely glycosylated form to the cell surface. *J. Biol. Chem.* 262:16618–16624.
33. Potma, E. O., W. P. de Boeij, …, D. A. Wiersma. 2001. Reduced protein diffusion rate by cytoskeleton in vegetative and polarized *dictyostelium* cells. *Biophys. J.* 81:2010–2019.
34. Derényi, I., F. Jülicher, and J. Prost. 2002. Formation and interaction of membrane tubes. *Phys. Rev. Lett.* 88:238101.
35. Heinrich, M., A. Tian, …, T. Baumgart. 2010. Dynamic sorting of lipids and proteins in membrane tubes with a moving phase boundary. *Proc. Natl. Acad. Sci. USA.* 107:7208–7213.
36. Pasternak, C., J. A. Spudich, and E. L. Elson. 1989. Capping of surface receptors and concomitant cortical tension are generated by conventional myosin. *Nature.* 341:549–551.
37. Jungbluth, A., V. von Arnim, …, G. Gerisch. 1994. Strong increase in the tyrosine phosphorylation of actin upon inhibition of oxidative phosphorylation: correlation with reversible rearrangements in the actin skeleton of *Dictyostelium* cells. *J. Cell Sci.* 107:117–125.
38. Heinrich, D., S. Youssef, …, G. Gerisch. 2008. Actin-cytoskeleton dynamics in non-monotonic cell spreading. *Cell Adhes. Migr.* 2:58–68.
39. Döbereiner, H.-G., B. Dubin-Thaler, …, M. P. Sheetz. 2004. Dynamic phase transitions in cell spreading. *Phys. Rev. Lett.* 93:108105–108109.
40. Cuvelier, D., M. Théry, …, L. Mahadevan. 2007. The universal dynamics of cell spreading. *Curr. Biol.* 17:694–699.
41. Pietuch, A., and A. Janshoff. 2013. Mechanics of spreading cells probed by atomic force microscopy. *Open Biol.* 3:130084–130094.
42. Bergert, M., S. D. Chandradoss, …, E. Paluch. 2012. Cell mechanics control rapid transitions between blebs and lamellipodia during migration. *Proc. Natl. Acad. Sci. USA.* 109:14434–14439.
43. Straight, A. F., A. Cheung, …, T. J. Mitchison. 2003. Dissecting temporal and spatial control of cytokinesis with a myosin II Inhibitor. *Science.* 299:1743–1747.
44. Shu, S., X. Liu, and E. D. Korn. 2005. Blebbistatin and blebbistatin-inactivated myosin II inhibit myosin II-independent processes in *Dictyostelium*. *Proc. Natl. Acad. Sci. USA.* 102:1472–1477.
45. Fukui, Y., A. De Lozanne, and J. A. Spudich. 1990. Structure and function of the cytoskeleton of a *Dictyostelium* myosin-defective mutant. *J. Cell Biol.* 110:367–378.
46. Fygenson, D. K., J. F. Marko, and A. Libchaber. 1997. Mechanics of microtubule-based membrane extension. *Phys. Rev. Lett.* 79:4497–4500.
47. Waterman-Storer, C. M., and E. D. Salmon. 1998. Endoplasmic reticulum membrane tubules are distributed by microtubules in living cells using three distinct mechanisms. *Curr. Biol.* 8:798–806.
48. Li, Y., R. Lipowsky, and R. Dimova. 2011. Membrane nanotubes induced by aqueous phase separation and stabilized by spontaneous curvature. *Proc. Natl. Acad. Sci. USA.* 108:4731–4736.
49. Andelman, D., T. Kawakatsu, and K. Kawasaki. 1992. Equilibrium shape of two-component unilamellar membranes and vesicles. *Europhys. Lett.* 19:57–62.
50. Seifert, U. 1993. Curvature-induced lateral phase segregation in two-component vesicles. *Phys. Rev. Lett.* 70:1335–1338.
51. Jülicher, F., and R. Lipowsky. 1993. Domain-induced budding of vesicles. *Phys. Rev. Lett.* 70:2964–2967.
52. Korlach, J., P. Schwille, …, G. W. Feigenson. 1999. Characterization of lipid bilayer phases by confocal microscopy and fluorescence correlation spectroscopy. *Proc. Natl. Acad. Sci. USA.* 96:8461–8466.
53. Roux, A., D. Cuvelier, …, B. Goud. 2005. Role of curvature and phase transition in lipid sorting and fission of membrane tubules. *EMBO J.* 24:1537–1545.
54. Parthasarathy, R., C.-H. Yu, and J. T. Groves. 2006. Curvature-modulated phase separation in lipid bilayer membranes. *Langmuir.* 22: 5095–5099.
55. McMahon, H. T., and J. L. Gallop. 2005. Membrane curvature and mechanisms of dynamic cell membrane remodelling. *Nature.* 438:590–596.
56. Kamal, M. M., D. Mills, …, J. Howard. 2009. Measurement of the membrane curvature preference of phospholipids reveals only weak

coupling between lipid shape and leaflet curvature. *Proc. Natl. Acad. Sci. USA.* 106:22245–22250.

57. Roux, A., G. Koster, …, P. Bassereau. 2010. Membrane curvature controls dynamin polymerization. *Proc. Natl. Acad. Sci. USA.* 107:4141–4146.

58. Mim, C., and V. M. Unger. 2012. Membrane curvature and its generation by BAR proteins. *Trends Biochem. Sci.* 37:526–533.

59. Yu, H., and K. Schulten. 2013. Membrane sculpting by F-BAR domains studied by molecular dynamics simulations. *PLOS Comput. Biol.* 9:e1002892.

60. Wienke, D. C., M. L. W. Knetsch, …, D. J. Manstein. 1999. Disruption of a dynamin homologue affects endocytosis, organelle morphology, and cytokinesis in *Dictyostelium discoideum*. *Mol. Biol. Cell.* 10: 225–243.

61. Rai, A., H. Nöthe, …, D. J. Manstein. 2011. *Dictyostelium* dynamin B modulates cytoskeletal structures and membranous organelles. *Cell. Mol. Life Sci.* 68:2751–2767.

62. Veltman, D. M., G. Auciello, …, R. H. Insall. 2011. Functional analysis of *Dictyostelium* IBARa reveals a conserved role of the I-BAR domain in endocytosis. *Biochem. J.* 436:45–52.

63. Heath, R. J. W., and R. H. Insall. 2008. *Dictyostelium* MEGAPs: F-BAR domain proteins that regulate motility and membrane tubulation in contractile vacuoles. *J. Cell Sci.* 121:1054–1064.

64. Heftmann, E., B. E. Wright, and G. U. Liddel. 1960. The isolation of Δ^{22}-stigmasten-3β-ol from *Dictyostelium discoideum*. *Arch. Biochem. Biophys.* 91:266–270.

65. Gilkes, N. R., and G. Weeks. 1977. The purification and characterization of *Dictyostelium discoideum* plasma membranes. *Biochim. Biophys. Acta.* 464:142–156.

66. Sorre, B., A. Callan-Jones, …, P. Bassereau. 2009. Curvature-driven lipid sorting needs proximity to a demixing point and is aided by proteins. *Proc. Natl. Acad. Sci. USA.* 106:5622–5626.

67. Kusumi, A., T. K. Fujiwara, …, K. G. N. Suzuki. 2012. Dynamic organizing principles of the plasma membrane that regulate signal transduction: commemorating the fortieth anniversary of Singer and Nicolson's fluid-mosaic model. *Annu. Rev. Cell Dev. Biol.* 28:215–250.

68. Heinemann, F., S. K. Vogel, and P. Schwille. 2013. Lateral membrane diffusion modulated by a minimal actin cortex. *Biophys. J.* 104:1465–1475.

69. Sun, Y., and D. G. Drubin. 2012. The functions of anionic phospholipids during clathrin-mediated endocytosis site initiation and vesicle formation. *J. Cell Sci.* 125:6157–6165.